

SCIENTIFIC REPORTS



OPEN

A record of igneous evolution in Elysium, a major martian volcanic province

David Susko¹, Suniti Karunatillake¹, Gayantha Kodikara², J. R. Skok³, James Wray⁴, Jennifer Heldmann⁵, Agnes Cousin⁶ & Taylor Judice¹

Received: 25 May 2016

Accepted: 22 January 2017

Published: 24 February 2017

A major knowledge gap exists on how eruptive compositions of a single martian volcanic province change over time. Here we seek to fill that gap by assessing the compositional evolution of Elysium, a major martian volcanic province. A unique geochemical signature overlaps with the southeastern flows of this volcano, which provides the context for this study of variability of martian magmatism. The southeastern lava fields of Elysium Planitia show distinct chemistry in the shallow subsurface (down to several decimeters) relative to the rest of the martian mid-to-low latitudes (average crust) and flows in northwest Elysium. By impact crater counting chronology we estimated the age of the southeastern province to be 0.85 ± 0.08 Ga younger than the northwestern fields. This study of the geochemical and temporal differences between the NW and SE Elysium lava fields is the first to demonstrate compositional variation within a single volcanic province on Mars. We interpret the geochemical and temporal differences between the SE and NW lava fields to be consistent with primary magmatic processes, such as mantle heterogeneity or change in depth of melt formation within the martian mantle due to crustal loading.

The lava fields surrounding Elysium Mons and its neighboring super-shield volcanoes, Albor Tholus and Hecates Tholus (Fig. 1), record some of the most recent volcanism on Mars^{1–4}. Most of the surface of Elysium Volcanic Province dates to the Amazonian period^{5–7} (beginning between 3.3 and 2.9 Ga), with a considerable areal extent of Late Amazonian age (beginning 0.6 to 0.3 Ga)⁴. Past work estimates that the age of the basement lava flows, the stratigraphically lowest and oldest we are able to observe in the region, date to ~ 4 Ga⁴. Other studies have identified late periods of volcanic activity in isolated areas of the southern portion of the Elysium Volcanic Province to extend to the last 250 Ma, including some remarkably young episodes as recent as 16.2–13.5 Ma, 4.3 Ma, and 3–2.5 Ma⁸. These dates highlight The Elysium Volcanic Province as particularly interesting, given its long and continuous history of volcanic activity. This long history suggests that these lavas could record varied magmatic evolution that can provide important constraints on the evolution of Mars as a geologically active and diverse planet. The Elysium Volcanic Province may also provide important insight for the geologic evolution of Amazonian terrains, given its geographic isolation in the northern lowlands away from other volcano-tectonic regions.

Mid-latitude (exclude latitudes poleward of $\sim \pm 45^\circ$) mapping of mass fraction distributions of the 9 elements: Al, Ca, Cl, Fe, H, K, Si, S, and Th, obtained from the γ spectral data from the Mars Odyssey Gamma and Neutron Spectrometer (GRS) instrument suite^{2,9–13}, showed a unique geochemical signature for Amazonian lava flows⁷ in the southeastern portion of the Elysium volcanic province (Fig. 1). Here, work by Karunatillake *et al.*² identified depletions in both K and Th (two elements characterized by the strongest geochemical affinity during igneous processes)^{9,14} by more than the combined standard deviation and typical standard error relative to their respective global averages. The depletion in these elements indicate that the southeastern lava fields are chemically anomalous when compared to the compositions of the martian mid-latitude regolith to decimeter depth scales¹¹. These anomalous geochemical signatures identify the Southeast Elysium lava fields as promising candidates for further geochemical investigation.

¹Department of Geology and Geophysics, Louisiana State University, Louisiana, USA. ²Department of Oceanography and Marine Geology, Faculty of Fisheries and Marine Sciences & Technology, University of Ruhuna, Matara, Sri Lanka. ³SETI Institute, California, USA. ⁴School of Earth and Atmospheric Sciences, Georgia Institute of Technology, Atlanta, GA, USA. ⁵NASA Ames, California, USA. ⁶Institut de Recherche en Astrophysique et Planétologie, Toulouse, France. Correspondence and requests for materials should be addressed to D.S. (email: Davidsusko@gmail.com)

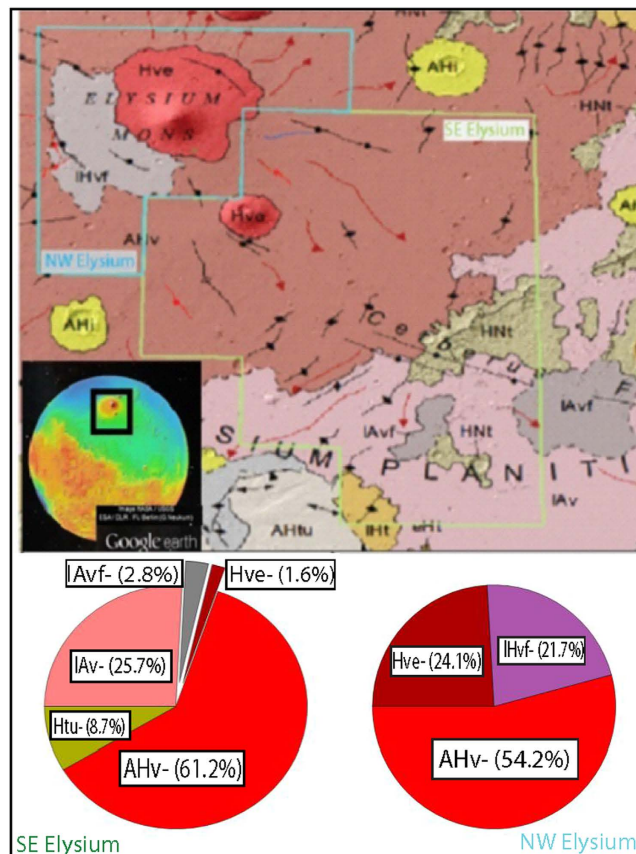


Figure 1. Location and geological setting of the Southeast (Green) and Northwest (Blue) Elysium lava fields with corresponding GRS pixels. Geology map adopted from the work by Tanaka *et al.*⁶ and made publically available at http://pubs.usgs.gov/sim/3292/pdf/sim3292_map.pdf. Inset image is a global reference map for Mars with overlain MOLA topography from Google Earth. The areal fraction of each unit within each region is quantified using ArcGIS software (pie charts). AHv is “Amazonian and Hesperian Volcanic unit”, IAv is “Late Amazonian Volcanic unit”, IAvf is “Late Amazonian Volcanic field unit”, IHvf is “Late Hesperian Volcanic Field unit”, Hve is “Hesperian volcanic Edifice unit”, Htu in the pie charts stands for “Hesperian Transition units” and is a combination of 3 geologic units: HNT (Hesperian-Noachian transition unit), IHt (Late Hesperian transition unit), and AHtu (Amazonian-Hesperian transition unit).

Recently, Baratoux *et al.*³ used γ data from the Northwest Elysium lava fields (Fig. 1) to investigate the thermal history of Mars during the Amazonian period. These authors investigated the composition of the lavas, and compared them to the compositions of Hesperian and Amazonian volcanic provinces elsewhere on Mars³. Abundances of SiO₂, FeO and ThO were used to estimate mantle potential temperature, degree of partial melting, and lithospheric thickness in correspondence with these volcanic provinces when these eruptions took place³. In this work, we compare the Southeast (SE) Elysium region to the Northwest (NW) Elysium region in order to constrain the spatial and temporal variation of composition of lava flows across a single martian volcanic province.

Previous investigations in the Radar Stealth region² suggests that data from the High Resolution Imaging Science Experiment (HiRISE), on board the Mars Reconnaissance Orbiter (MRO), can lead to inferences about the physical properties of surface-to-subsurface material. In this work we use HiRISE imagery to complement in our interpretation of geochemical signatures.

Cerberus Fossae, an area overlapping the southern portion of the chemically anomalous region in SE Elysium, contains evidence of chemical layering involving volatile elements in the subsurface, potentially due to complex interactions among lava flows, volcanic aerosols and eolian sediment¹⁵. Morphologies, such as mesas and other related features in close proximity to Cerberus Fossae, have been ascribed to phreatomagmatism^{1,16,17}, lava-water interactions¹⁸ and relict ice floes^{19,20}. Observations of patterned ground with a remarkable similarity to terrestrial periglacial environments²¹ also suggest the likelihood of geologically recent aqueous processes. All these processes could explain some of the observed chemistry. However, radar sounding data appear consistent with interbedded lava flows and weakly compacted sediments or porous rocks²².

Pure water is unstable on the surface of Mars^{23–25}. Brines, however, could have been free-flowing on the surface and could still be present in subsurface reservoirs of Mars²⁶, and thus could be thought of as agents for alteration of surface rock. Common secondary minerals on Mars, such as Ca- and Mg- Sulfates and Fe-Oxides could be deposited by low pH, sulfur-rich, aqueous solutions in very low water-to-rock ratio, and subsequently, limited

Al-mobilization conditions²⁷. Evaporite minerals, such as Halite (NaCl) and anhydrite (CaSO₄), could have precipitated following evaporation of highly saline aqueous solutions. If the volatiles detectable by the GRS, (S, Cl, and H₂O) are enriched in either SE or NW Elysium, this could support the presence of such minerals at regional scales.

In addition to observations made by orbiting spacecraft, we make comparisons between the regional chemistry in Elysium and *in situ* samples analyzed from rover landing sites on Mars and the martian meteorites. The compositional data for several martian meteorites as well as *in situ* samples from Gusev Crater, analyzed using the Alpha Particle X-ray Spectrometer (APXS) onboard the MER Spirit Rover, are used for comparison with the γ data. The martian meteorites, which have been used in the past to model the compositions for bulk silicate Mars^{28,29}, provide the most detailed information about the martian mantle's evolution and magmatic differentiation of any data set available to us. In order to better understand igneous alteration trends, which may be applicable to the Elysium Volcanic Province, we use previously categorized *in situ* rock samples from Gusev, which have been divided into unaltered and altered igneous samples^{30–33}. In this study, we were able to rule out the presence of a secondary geochemical signature, and establish igneous processes as the principal factor controlling Elysium's anomalous compositions.

Geologic Setting and Characteristic Geomorphology

The Elysium lava flows erupted from the edifices of the three super-shields, from volcanic fissures, and from at least 22 topographically low shield volcanoes scattered across the Elysium Volcanic Province⁸. Using the most recent mapped geologic units of Mars^{6,7}, we quantified the areal fraction of each geologic unit comprising both NW and SE Elysium (Fig. 1). The SE Elysium region (1.37×10^6 km² in areal extent) is dominated by Amazonian volcanic units, which comprise nearly 90% (1.23×10^6 km²) of its areal fraction. The most abundant unit type is the Amazonian-Hesperian volcanic unit (AHv), making up more than 60% (8.22×10^5 km²) of the surface (Fig. 1). The AHv contains low viscosity flood lavas and stacked, gently sloping, lobate flows of highly variable ages, which are sourced from vent systems and local fissures rather than large volcanic edifices⁶. Late Amazonian volcanic units and volcanic fields, LAV and LAVf respectively, make up nearly 30% (4.11×10^5 km²). They contain planar deposits consisting of troughs, ridges, and platy textures which we identified in HiRISE image Fig. 2F. These units are young, and include pristine flows and occasional sinuous lava channels (Fig. 2D). The rest of the region is made up of Hesperian transition units (Htu) and the Hesperian Volcanic Edifice (HVe) of the super-shield Albor Tholus⁶ (Fig. 1).

Several Hesperian geologic units are mapped in the NW region of Elysium (5.06×10^5 km² in areal extent)^{6,7}. While the majority of the region is characterized as AHv (~54% of the surface, or 2.72×10^5 km²), a significant portion (~22% or 1.11×10^5 km²) of the surface is covered by the Late Hesperian volcanic field unit (IHvf). The IHvf unit is hundreds of meters thick and is made up of far flowing, low viscosity lavas which are locally modified by troughs and fissures⁶, such as those shown in Fig. 2C. The remaining ~24% of the NW region (1.21×10^5 km²) is covered by the HVe unit (~24%), which makes up the edifice of the super-shield volcano Elysium Mons⁶. These Hesperian units, which did not experience the same Amazonian volcanic resurfacing events as SE Elysium, contribute substantially to the observed geochemistry in the NW region.

Morphologies indicative of effusive volcanic eruptions are observed throughout both the SE and NW Elysium regions. Figure 2 shows some representative morphologies. In terrestrial settings, basaltic magma often generates effusive eruptions that build deep, sinuous lava channels⁵, which are analogues to features shown in various HiRISE images. Terrestrial observations, suggesting greater flow distance with lower viscosities remain applicable to the Elysium lava flows (Fig. 2A). These images also show other low viscosity morphologies such as infilled craters, lobate flows, and platy ridge flows. Pa'hoehoe lava features form when low viscosity lava cools and becomes more viscous, this results in an over-folding, ropy morphology. Analogous features are present within the SE Elysium region (Fig. 2E and H). The crater shown in Fig. 2C, located in NW Elysium, is not an impact crater, but is thought to be a collapse feature of a lava tube, as evident by the presence of scalloped walls and the lack of ejecta blanket, raised rim, or central peak¹. This collapse feature exposes layered lava flows, effectively revealing the stratigraphic record of lava flows that have created the Elysium Volcanic Province over its geologic history^{4,8}.

Other morphologies may suggest the presence of alternative geologic processes taking place concurrently with these lava flows. Figure 2H shows rootless cone structures, identifiable based on their clustered behavior on top of lava flows and the lack of extruded material around their circular bases¹⁸. These features have been interpreted to be a product of lava flow emplacement over a hydrated surface¹⁶. The local ground water or ice is volatilized by the hot, flowing, lavas and creates a phreatomagmatic explosion resulting in these cones^{16,18,34,35}. These features, also visible roughly 1 km south of the infilled crater in Fig. 2G, were identified in the SE Elysium region, but were not observed in the NW.

Results

While past analysis has looked at the ages of Elysium Planitia broadly⁴ or on a more localized basis^{8,35}, we sought to estimate the average age of all the lava flows within surface areas of similar regional geochemistry within Elysium^{2,3}. The total number of craters (N) greater than 1 km in diameter was found to be N = 925 for the SE Elysium region and N = 482 for the NW. The cumulative crater frequency reveal the average age of the surface in SE Elysium province is 2.59 ± 0.08 Ga, while the surface in NW Elysium is estimated to be 3.44 ± 0.02 Ga (Fig. 3). Both dates are comparable to previous studies of the ages of various lava flows within Elysium, which estimated the oldest lava flows to range between 4 and 2 Ga⁴.

Ratio bound box plots² (Methods) show meaningful differences in compositional distributions between the SE and NW regions. In this work, an elemental abundance in a region "A" is referred to as a "major" enrichment or depletion, relative to a region "B", when the lower (25thtile/75thtile) or upper (75thtile/25thtile) bound,

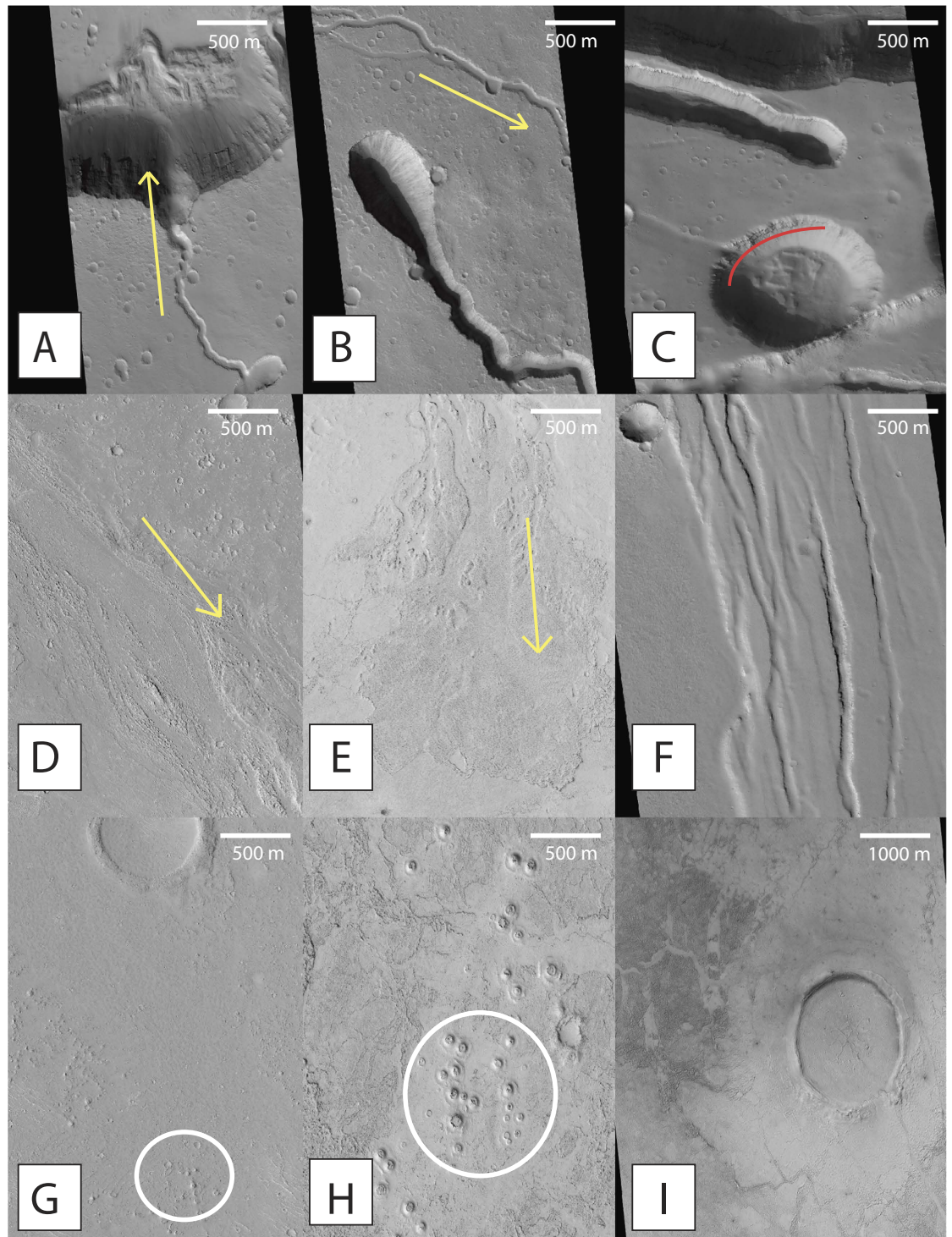


Figure 2. Selected HiRISE imagery from both SE and NW Elysium regions. (A) ESP_022915_2070 (26.949°N, 142.844°E) shows flows down a crater slope in NW Elysium. (B) ESP_013157_2015 (21.498°N, 149.738°E) shows lava flows on the south flank of Elysium Mons within NW Elysium. (C) PSP_004046_2080 (27.49°N, 143.21°E) shows fissures and pit crater collapse feature of lava tubes in the NW region. The collapse of the lava tube has exposed stratified lava flows. (D) ESP_037802_1880 (8.1°N, 154.7°E) shows lava channels and accompanying lava levees within SE Elysium. (E) PSP_005984_1850 (5°N, 156.4°E) shows pa'hoehoe style flows and a lava-draped channel at its terminus within SE Elysium. (F) ESP_014278_2050 (24.71°N, 143.6°E) shows the lava flow boundary between separate geologic units HVe and IHvf in the NW region. (G) ESP_028466_1955 (15.22°N, 162.45°E) shows an image from the SE with an infilled crater in the top half of the image and rootless cones (circled) in the bottom half. (H) ESP_012524_1855 (5.58°N, 153.07°E) shows more prominent rootless cone structures as well as abundant Pa'hoehoe analog style flows within SE Elysium. (I) ESP_034967_1885 (8.48°N, 149.19°E) shows a large crater infilled by the lava flows from SE Elysium. North is up in all pictures. The yellow arrows represent inferred direction of flows.

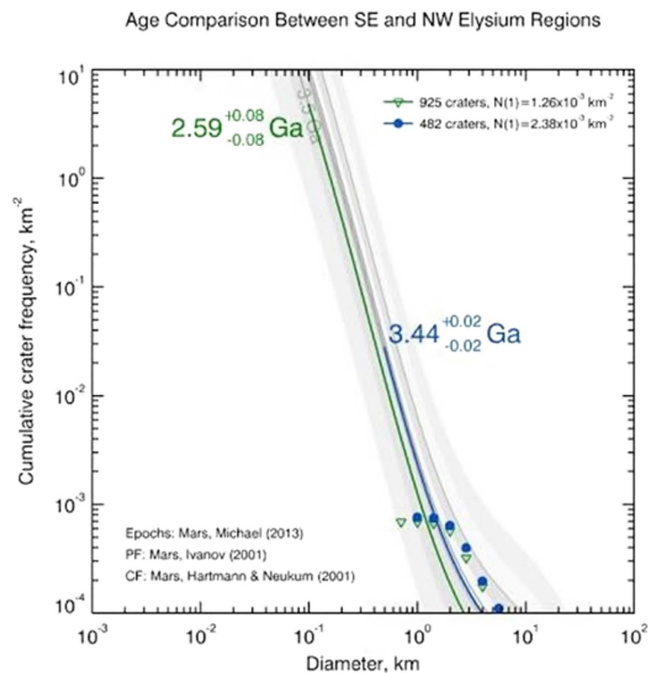


Figure 3. CraterStats2 results for planetary surface age dating using crater counting^{7,55}. 925 craters greater than 1 km in diameter were identified for the SE Elysium region, while only 482 craters of the same size were identified in the smaller NW region. This figure plots Diameter of Craters vs Cumulative Crater Frequency. Southeast Elysium (green) is estimated to be younger at 2.59 ± 0.08 Ga and Northwest Elysium (blue) older at 3.44 ± 0.02 Ga.

respectively, surpasses unity. In turn, the enrichment or depletion is considered “minor” when the ratio of median surpasses unity but the lower or upper bounds do not. An abundance is considered similar between the two regions if the ratio of the 50thtile/50thtile is within one standard error. We list the error-bound median ratio in parenthesis following the element.

The first ratio bound box plot compares the regional geochemistry of the SE Elysium region to the composition of the average martian crust (Fig. 4A). In addition to the previously identified major depletions of K (0.72 ± 0.05) and Th (0.63 ± 0.05)², this region differs significantly from the typical martian crust in several elements detectable with γ spectra, as shown by Fig. 4A. The region has a minor depletion in Si (0.97 ± 0.02) and Al (0.91 ± 0.05), while Ca (1.26 ± 0.10) and Fe (1.11 ± 0.08) display major enrichments throughout the region. For example, the lowest values, represented in the 25th percentile, of Ca and Fe, exceed most of the highest values, represented in the 75th percentile, of the martian crust. This amounts to enrichments in Fe to over 16% of the bulk composition in some parts of the region, which is significant, considering that average for the martian crust is only $12.6 \pm 0.7\%$. A major regional enrichment in S (1.14 ± 0.04) is also observed.

Mars has a history of global-scale dust storms which mobilize layers of high albedo fine material of few microns to tens of micron size scale (i.e., dust) across the planetary surface³⁶. Elysium in particular has a thick layer of this dust³⁷. We renormalize the γ derived geochemistry to a volatile and “mobile” element-free basis in order to ensure the compositions investigated in Elysium represent the igneous components at the surface, rather than those affected by interference from the dust. The normalization factors were calculated for each pixel using the standard equation $100/(100 - [\text{H}_2\text{O}] - [\text{SO}_3] - [\text{Cl}])$ ¹⁰. A constant oxidation state of +6 is assumed for S when converting to SO_3 ¹⁰. The results (Fig. 4B) reveal that the volatile-free compositions show the same relative trends between the SE and the martian crust as the volatile-bearing compositions, indicating the compositions are cation-conserving²⁷, and volatiles merely dilute the abundances of the major elements, rather than dominate a surficial layer.

Compared with the average martian crust, the NW Elysium region has minor enrichments in Ca (1.13 ± 0.03) and H_2O (1.11 ± 0.07), as well as a major depletion in Si (0.96 ± 0.01) and a major enrichment of S (1.11 ± 0.02). The NW region also shows a minor depletion in Al (0.80 ± 0.08) and major depletions in K (0.79 ± 0.02) and Th (0.81 ± 0.05). These results are shown in ratio bound box plot for Fig. 4C.

When compared to one another, the two regions of the Elysium Volcanic Province reveal several interesting geochemical trends (Fig. 4D). The SE Elysium region displays a minor enrichment of Ca (1.11 ± 0.07) and major enrichments in Al (1.34 ± 0.08) and Fe (1.09 ± 0.08). Both regions have nearly identical abundances of Si (1.02 ± 0.03). Despite both regions having major depletion in the high spectral precision elements, K and Th, relative to the martian crust, the depletion is even more significant in the SE region, which shows a major depletion relative to the NW.

We use molar ternary plots^{27,31,33,38} to further our geochemical analysis of the Elysium provinces and test whether aqueous alteration could explain the observed geochemical anomalies. We selected a ternary diagram

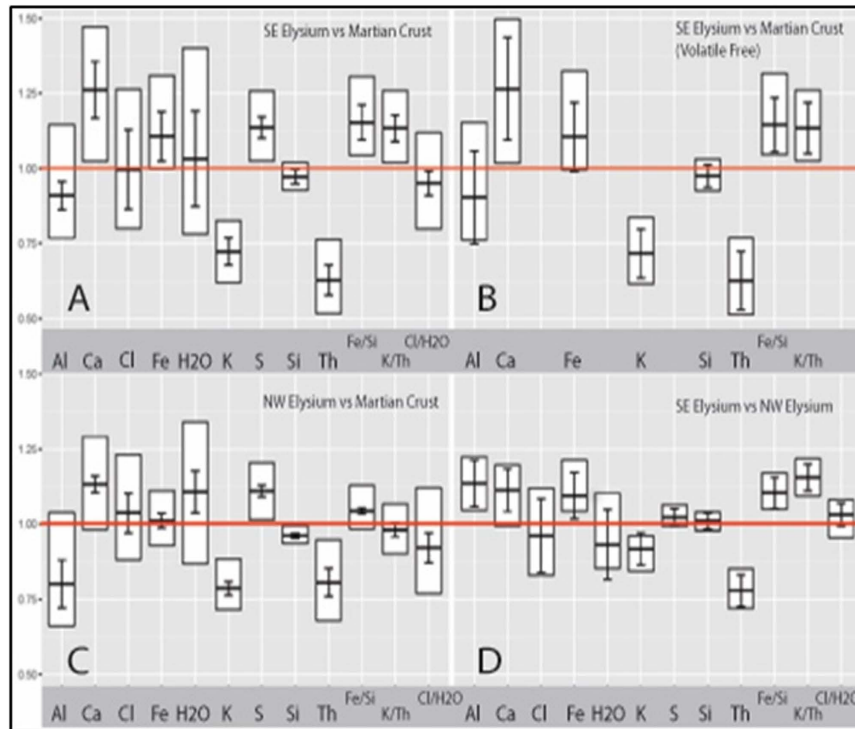


Figure 4. Ratio bound box plots indicate compositional ratios of one target region to another as 75th/25th percentile, 50th/50th percentile, and 25th/75th percentile for the mass fraction of the elements: Al, Ca, Cl, Fe, H₂O, K, S, Si, Th, and the ratios of Fe/Si, K/Th, and Cl/H₂O. Deviation of the median ratio from unity would suggest tentative compositional distinctness, while the lack of overlap with unity for a given box would show a significant change, even for small relative differences. Error bars were calculated as the uncertainty of the median average deviations (MAD) using the equation $MAD = \text{median} [|X_i - \text{median}(X_i)|]$, where median (X_i) is the median of all values X_i ⁵⁴. The MAD of a set of values is particularly robust and is more resilient against outliers in the data when compared to the standard deviation. Red lines highlight the 1 to 1 ratio, values below the line represent depletion, while values above represent enrichments. (A) Chemical differences between the Southeast Elysium region and the chemical average for the martian crust. (B) SE Elysium vs martian crust, normalized for an observed volatile-free basis, removing Cl, S, and H₂O from the bulk composition. (C) NW Elysium Chemical province vs martian crust. This plot highlights the similarities in trends away from the martian crust compositions for both the NW and the SE regions (shown in a). (D) NW Elysium Chemical province vs the SE Elysium chemical province, showing the differences between regions, most notably in Ca, Fe, K, and Th.

which has been used to describe the aqueous weathering trends of olivine-bearing basalts, given their pervasiveness in the martian crust, under both moderate pH regimes of typical terrestrial settings³⁸ and low pH conditions, with low water to rock ratios, where most chemical weathering processes on Mars occur²⁷. The apices of this ternary are (Al₂O₃) – (CaO + Na₂O + K₂O) – (MgO + FeO) [A-CNK-MF] (Fig. 5). For the moderate pH conditions on Earth, altered rocks progress from below the feldspar-olivine tie-line, which connects the pure end-member compositions of general feldspar [(K,Na,Ca)(Al,Si)₂Si₂O₈] and olivine [(Mg,Fe)₂SiO₄], toward the Al₂O₃ composition^{38,39}. This terrestrial trend is shown by the black “weathering” arrow in Fig. 5. The second trend-line corresponds to the results from the alteration of synthetic martian rocks under low pH laboratory conditions, with the altered rock progressing toward to A-CNK edge of the ternary and the alteration fluid progressing toward to MF apex²⁷. Even though the ternary plots have both Na₂O and MgO components, these oxides lack the associated γ -derived chemical data. Consequently, we use the method by Baratoux *et al.*⁴⁰ to estimate Na₂O and MgO mole fractions (Methods).

Figure 5 shows the majority of the Elysium chemical provinces’ pixels plotting directly on the low pH system aqueous alteration trend line³². Pixels from both the NW region (blue) and the SE region (red) overlap and plot near the alteration under low pH trend line (dashed line), close to the unaltered rock composition (white disk), away from the altered composition of basalts (orange disk). The martian meteorites, generally plot below the trend line for low pH aqueous alteration, closer to the CNK-MF edge of the ternary. The APXS-analyzed *in situ* rocks from Gusev Crater generally plot between the low pH aqueous alteration trend line and the Feldspar-Olivine Tie-Line. The unaltered igneous samples plot closer to the martian meteorites, while the altered rocks plot above them, closer to the feldspar-olivine tie-line. The NW and SE Elysium pixels plot on the trend line between the martian meteorites and the unaltered Gusev igneous rock.

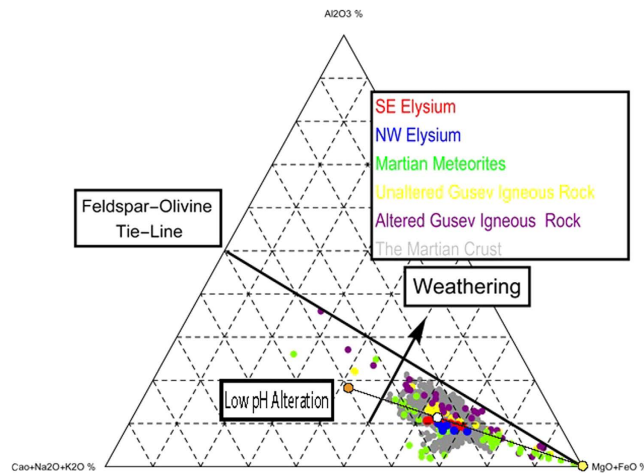


Figure 5. Ternary plot of $(\text{Al}_2\text{O}_3) - (\text{CaO} + \text{Na}_2\text{O} + \text{K}_2\text{O}) - (\text{MgO} + \text{FeO})$ as a proxy for the index of alteration for martian rocks. The black ellipse represents the range of values for the martian crust as detected by GRS. Open system aqueous alteration trend is shown with the black line, with altered rock (left circle), unaltered rock (middle), and alteration fluid (right). This line corresponds to the results from the alteration of synthetic martian rocks under low pH laboratory conditions by Hurowitz and McLennan²⁹. Plots the pixels from both SE (red) and NW (blue) Elysium vs the martian meteorites (green), unaltered Gusev igneous rock (yellow), altered Gusev igneous rock (purple) and the rest of the GRS data (gray). The data sets form a trend in the direction of more exposure to alteration effects, with the martian meteorites representing compositions of little-to-no alteration, and the altered Gusev samples representing the most heavily altered igneous compositions.

Discussion

In this work, we identify a compositional shift temporally and spatially across the Elysium Volcanic Province from the older NW region (3.44 ± 0.02 Ga) to the more recent SE region (2.59 ± 0.08 Ga). Through the convergence of multiple data sets, we quantify the compositional changes in lavas of variable ages across the province. Our results indicate that the unique geochemistry of the Elysium Volcanic Province represents igneous processes as opposed to secondary aqueous alteration of the surface or interference from eolian superficial dust.

The resulting $0.85 \pm .08$ Ga difference between the SE and NW Elysium regions estimated by crater counting provides the province with a record of varied magmatic compositions over its geologic history. This in turn, helps to constrain the evolution of Mars as a geologically active planet. The Hesperian/Amazonian temporal boundary is estimated to be between 3.3 to 2.9 Ga, but could also vary as much as from 3.4 to 2.0 Ga due to poorly constrained martian cratering and erosional rates during the time⁴¹. With this chronology in mind, the SE Elysium region is decidedly Amazonian, while the older NW Elysium province falls at end of the late Hesperian era, just prior to the Hesperian/Amazonian Boundary. Consequently, prior analyses by Baratoux *et al.*³ that focused exclusively on the NW region, may not represent the thermal history of the Elysium Volcanic Province during the Amazonian period as directly as the SE province.

The NW region is depleted in Al, Ca, and Fe compared to the SE region, while K and Th show significant depletions in the younger flows. In order to compensate for the observed depletions in Al, Ca, and Fe, an unreported major (>10%) rock-forming element must be enriched in the NW to sum the total oxide mass fractions detected by the GRS up to unity for mass balance purposes. The only major rock-forming element not reported by the GRS is Mg, making it a reasonable candidate for the majority of the missing mass fraction. These differences in major element abundances between the two regions have major implications for time dependent changes to the composition of the martian mantle from the late Hesperian to the Amazonian periods.

Elemental ratios can be used to assess the likelihood of secondary geologic processes. Elysium, like much of the northern mid-latitudes, has a surficial layer of fine material dominated by tens of microns grain size, or “dust”^{42,43}. This dust is characteristically bright, having high albedo and low thermal inertia, and has been found to partially dominate the geochemical signature of large regions of the planet⁴⁴. Bright dust at the MER rover sites, Gusev and Meridiani, was analyzed using the APXS instrument and found to contain elevated abundances of the more mobile and volatile elements, S and Cl, relative to darker, less mobile soil and rock⁴⁵. Evidence of abundant hydrated minerals within the soils was also found using the MER rovers’ MiniTES instrument⁴⁶. An abundance of dust could cause the elevated levels of S in the SE and both S and H₂O in the NW^{46,47}. If the primary source of volatile elements at Elysium is attributed to a layer of globally-sampled dust deposited by atmospheric processes, then the chemical province should yield a Cl/H₂O ratio similar to the global average. Rather, we observe a lower Cl/H₂O ratio in both the SE and NW regions relative to the martian crust (Fig. 4A and C). More likely, the distinct Cl/H₂O ratio and enrichment in S reflect the volatile content of the magma which formed the Elysium Volcanic Province, as these volatiles are readily sourced from volcanic degassing¹².

Past work has described dust within the most heavily mantled regions of Mars to be enriched in K and Th rather than depleted⁴⁴. These heavily mantled regions, which include Arabia, Tharsis, and Amazonis, are chemically distinct from one another, indicating that the γ signature is reflective of locally, rather than globally, derived

material^{11,44}. If this is the case in Elysium, even if the GRS is sampling the signature from the dust, it still reflects the igneous compositions of the region. If the γ signature had been influenced by the sampling of a thick layer of volatile-enriched dust on top of the bulk basaltic crust, the renormalizing to a volatile-free basis would have caused an apparent enrichment in the remaining elements. The volatile-free ratio bound box plot (Fig. 4B) comparing SE Elysium to the martian crust does not reveal any deviation from the relative abundance trends compared to the bulk compositions. This supports the idea that the GRS is primarily sampling the bulk basaltic rock composition.

Effusive lava flows, which result from hot magma outpouring onto the surface, can be greatly influenced by H₂O in its source; even just a few ppm of water in the lava could greatly reduce its viscosity⁵, and NW Elysium shows a minor enrichment of H₂O in the γ data relative to the martian crust. As mentioned previously in this work, morphologies characteristic of effusive flows such as ropey, lobate textures, sinuous channels, and lava tubes dominate the landscape across both regions of Elysium. The rootless cone structures within SE Elysium could indicate a wet environment with higher than average water-to-rock ratios on the surface during the time of emplacement of these lavas, but they do not appear to be widespread enough to dominate regional geochemistry. In addition to morphology, calculations done by prior work for the temperature of NW Elysium magmas also favor a relatively hot source, with mantle potential temperatures of 1405 °C, the highest of any Amazonian volcanic province analyzed by that work³. This high temperature would suggest a deep mantle origin and would agree with the undepleted magma compositions with high abundances of volatiles, such as H₂O, that are observed in the γ data.

The temporal variation between the two regions is consistent with magmatic variability and provides a degree of insight into the igneous evolution of the Elysium Volcanic Province. The observed geochemical trends suggest a difference in source signature between the older NW region and younger SE region (Fig. 4). Two possible interpretations arise to explain these temporal variations in geochemistry. The first is that of a heterogeneous mantle, with pockets of distinct compositions contributing to the geochemical signatures we observe on the surface at different periods in martian history. Multiple models exist to describe how the martian mantle might be compositionally heterogeneous both laterally and vertically. The possibility of a whole-mantle magma ocean on early Mars has been speculated. The model predicts solidification of multiple zones of cumulates in the mantle at different depths, which eventually differentiate into distinct lateral components when the deeper cumulates rise and settle at neutral buoyant forces nearer to the shallow zone⁴⁸. This mantle overturn leads to lateral heterogeneity, with multiple zones of cumulates of different densities, within mantle sources. Differences in mineral content is expected to be observed in the eruptions from these sources, with regions of dominated by specific minerals, with lower density cumulates being enriched in MgO and higher density cumulates being enriched in FeO⁴⁸. It is worth noting that Fe, which other than Si, is the most abundant element detectable by the GRS and shows significant variability between the two regions. Fe may prove to be a more useful indicator of mantle overturn at regional scales across Mars.

Recent work by Balta & McSween⁴⁹ has described a separate model for martian mantle evolution which could lead to source heterogeneity. This model proposes that older Hesperian volcanoes were sourced from a portion of the upper depleted mantle, while the younger Amazonian volcanoes were occasionally sourced from upwelling from a deeper undepleted portion of the mantle. This upwelling provides the surface with water-rich, shergottite-like compositions⁴⁹. These lavas of distinct age and composition within Elysium could potentially represent a regional expression of this global mantle evolution. This is unlikely, however, because the compositions observed in the two regions of Elysium (i.e. relative enrichment in Fe and H₂O for the younger SE region) do not match expectations of the model by Balta & McSween⁴⁹, which predicts higher concentrations of Th and H₂O and depletions in Fe for the younger eruptions.

The second interpretation of possible igneous processes exists as a change in depth of the melt formation in the mantle beneath the Elysium Volcanic Province. This is made possible by a model which predicts continual mantle plumes rising to the surface throughout Elysium's lengthy eruptive history during the late Hesperian and Amazonian Eras¹. The loading of the lithosphere by the formation of the super-shields could cause an increase in pressure on the mantle source over time, depressing the geothermal gradient. This increase in pressure would be accompanied by a decrease in degree of partial melting and an increasing depth of melt formation. The younger volcanism in the SE, where lithospheric thickness is considerably lower⁴⁰, would take place with lower pressures and at shallower depths. With distinct depth to melt formations between the Hesperian and Amazonian, magmas erupted with notably different abundances of elements. This is supported by the compositional distinctness between the NW region and SE region of several major and minor elements (Fig. 4D), most notably Th and Fe. The higher concentration of Th in NW Elysium suggests a lower degree of partial melting in the mantle source³, while the elevated Fe abundance in the SE is likely indicative of a change to a shallower source depth⁵⁰ in SE Elysium.

Based on our results, the geochemistry seems most consistent with a model for the change in the depth of melt formation in the mantle beneath the Elysium Volcanic Province. This conclusion has major implications for the history of martian mantle evolution, such as how volcanic provinces were built up over time, and motivates future investigations into this province. Petrologic modeling techniques using pMELTS and SPICES programs on the bulk silicate compositions of Mars proposed by Taylor²⁹ might help us to constrain how the compositions of volcanic provinces changes with variable pressures and degrees of partial melting.

Methods

In order to investigate a potential sub-era variation in volcanism, we use mapped geologic units in the SE and NW Elysium chemical provinces^{6,7} and crater counting techniques to estimate crustal ages for each area. ArcGIS software in conjunction with the Mars Orbiter Laser Altimeter (MOLA) data was used to highlight the areas of interest. These highlighted areas were saved as shape files. Within each area, craters were marked by defining

three points around the rim, before being subsequently exported to the CraterStats2 program. The program then generated a crater diameter vs cumulative crater frequency graph in order to calculate the estimated ages for the two provinces⁴¹.

In the present work, the data from all γ pixels in the martian mid-latitudes, other than those identified as the two Elysium Chemical Provinces, collectively represent the bulk composition of the martian crust, down to depths of several decimeters²⁹. Each GRS pixel has a spatial resolution of several hundred km². The small fractional area of Mars occupied by the Elysium chemical provinces also ensures that other data pixels approximate the bulk crust characterized before by Taylor *et al.*¹⁴ and McSween *et al.*⁵¹. Specifically, while the extent of the SE and NW Elysium chemical provinces (Fig. 1) are about 1.37×10^6 km² and 5.06×10^5 km², respectively, they constitute a sufficiently small area to ensure that their exclusion from the bulk crustal values does not make the bulk crustal estimate unreliable. Their exclusion enables unambiguous insight into compositional trends distinct from those in the typical martian crust. For our investigations using the γ data, we use the maps constructed from cumulative gamma spectra mapping periods extending through 2009, refining the older compositional data for greater accuracy and precision than those used in Karunatillake *et al.*². We also include previously unreported chemical maps for the elements Al and S. Our chemical data exclude latitudes poleward of $\sim \pm 45^\circ$, where high H concentrations cause both mass dilution effects and inaccuracies in γ spectrum-to-elemental mass fraction derivation^{2,11}. We use mid-to-low latitudinal mass fraction maps generated from the GRS instrument. We bin each of the maps from their original dimensions to $5^\circ \times 5^\circ$ pixel size. This serves to reduce spatial uncertainty associated with the reduced degrees of freedom from spatial autocorrelation^{52,53}. The radioactive elements K and Th are the two elements with the finest γ spatial resolution, owing to the orbiting instrument's detection of natural radioactive decay and independence from neutron-driven scatter and capture processes, unique among the majority of elements detected by the GRS instrument¹¹. It is for this reason that K and Th are the primary elements utilized for interpretation of geologic processes.

In the ratio bound box plot method, the ratio of the 25th percentile of a particular element's reported mass fraction within a region "A" to the 75th percentile of values for the same element within a region "B" would bound how low the values are within "A" relative to those present within "B". The ratio of the 25th%tile of "A"/75th%tile of "B" is represented by the bottom of each "box" in Fig. 4. Likewise, the ratio of the 75th percentile of region "A" compared to the 25th percentile within "B" bounds how high the values within "A" can be relative to those within "B". The ratio of the 75th%tile of "A"/25th%tile of "B" is represented by the top of each "box" in Fig. 4. The ratio of the 50th percentile of "A" to the 50th percentile of region "B" (ratio of medians) indicates how the typical compositions compare with one another⁵³, represented in the mid-section of each "box". The error bars were propagated for the ratio of the 50th%tile/50th%tile using the median absolute deviations (MAD) for each element in both regions, using the equation $MAD = \text{median} [|X_i - \text{median}(X_i)|]$ ⁵⁴, where median (X_i) is the median of all values in X_i . These error bars are statistically robust and typically overcompensate the uncertainty of the values of various %tiles. When constructing the ratio bound box plot in Fig. 4B, the normalization to a volatile-free basis was done on a pixel-by-pixel. This prevented the normalization from being effectively canceled out as a common denominator in the ratios.

The method for MgO abundance calculation used in this study uses oxide ratios reported from martian meteorites to calculate values for the following oxides: Na₂O ($\text{Na}_2\text{O}/\text{TiO}_2 = 1.374 \pm 0.337$), TiO₂ ($\text{TiO}_2/\text{P}_2\text{O}_5 = 1.151 \pm 0.265$), P₂O₅ ($\text{P}_2\text{O}_5/\text{K}_2\text{O} = 4.297 \pm 0.931$), and MnO ($\text{MnO}/\text{FeO} = 0.025 \pm 0.001$)⁴⁰. Their calculated values were added to the oxide values converted from the elemental γ spectral data (Al₂O₃, CaO, FeO, SiO₂, and K₂O) and normalized to be volatile-free. The subsequent value was subtracted from 100, and the remaining value was assumed to represent the MgO content, as Mg is the only remaining major rock forming element. Major caveats exist in this calculation and uncertainties are very large. To partially address these concerns, we ignore any GRS pixels for which these calculations return Mg# < 40 or > 70, as it is not consistent with an igneous crust from an initial mantle composition of roughly Mg# 75^{28,40}. The Mg# was calculated by using the mole fraction of the oxides MgO and FeO with the formula $[\text{Mg}\# = 100 * (\text{MgO}/(\text{MgO} + \text{FeO}))]$.

The oxide data used in the construction of the geochemical ternary plot for the martian meteorites were obtained by previous studies in laboratory settings. They were accessed online from the publicly available Martian Meteorite Compendium (<http://curator.jsc.nasa.gov/antmet/mmc/>). Similarly, the *in situ* samples analyzed with the Alpha Particle X-ray Spectrometer (APXS) from the MER rovers (Spirit) at Gusev Crater were obtained online, publicly available at MERAnalyst, (<https://an.rsl.wustl.edu/>), part of NASA's Planetary Data Systems interface.

References

- Dohm, J. M. *et al.* Recent geological and hydrological activity on Mars: The Tharsis/Elysium corridor. *Planetary and Space Science* **56**, 985–1013 (2008).
- Karunatillake, S. *et al.* Chemically striking regions on Mars and Stealth revisited. *Journal of Geophysical Research* **114**, E12001 (2009).
- Baratoux, D., Toplis, M. J., Monnereau, M. & Gasnault, O. Thermal history of Mars inferred from orbital geochemistry of volcanic provinces. *Nature* **472**, 338–41 (2011).
- Hartmann, W. K. & Berman, D. C. Elysium Planitia lava flows' Crater count chronology and geological implications. *Journal of Geophysical Research* **105**(15), 011–15,025 (2000).
- Grott, M. *et al.* Long-Term Evolution of the Martian Crust-Mantle System. *Space Science Reviews* **174**, 49–111 (2012).
- Tanaka, K. L. *et al.* Geologic Map of Mars. *US Geological Survey Geologic Investigations Map* **3292**, doi: 10.3133/sim3292 (2014).
- Tanaka, K. L., Robbins, S. J., Fortezzo, C. M., Skinner, J. a. & Hare, T. M. The digital global geologic map of Mars: Chronostratigraphic ages, topographic and crater morphologic characteristics, and updated resurfacing history. *Planetary and Space Science* **95**, 11–24 (2014).
- Vaucher, J. *et al.* The volcanic history of central Elysium Planitia: Implications for martian magmatism. *Icarus* **204**, 418–442 (2009).
- Gasnault, O. *et al.* Quantitative geochemical mapping of martian elemental provinces. *Icarus* **207**, 226–247 (2010).

10. Taylor, G. J., Martel, L. M. V., Karunatillake, S., Gasnault, O. & Boynton, W. V. Mapping Mars geochemically. *Geology* **38**, 183–186 (2010).
11. Boynton, W. V. *et al.* Concentration of H, Si, Cl, K, Fe, and Th in the low- and mid-latitude regions of Mars. *Journal of Geophysical Research* **112**, E12S99 (2007).
12. Gaillard, F., Michalski, J., Berger, G., McLennan, S. M. & Scaillet, B. Geochemical Reservoirs and Timing of Sulfur Cycling on Mars. *Space Science Reviews* **174**, 251–300 (2012).
13. Feldman, W. C. *et al.* Vertical distribution of hydrogen at high northern latitudes on Mars: The Mars Odyssey Neutron Spectrometer. *Geophysical Research Letters* **34**, L05201 (2007).
14. Taylor, G. J. *et al.* Variations in K/Th on Mars. *Journal of Geophysical Research* **112**, E03S06 (2006).
15. Diez, B. *et al.* Contribution of Mars Odyssey GRS at Central Elysium Planitia. *Icarus* **200**, 19–29 (2009).
16. Burr, D. M., Grier, J. a., McEwen, A. S. & Keszthelyi, L. P. Repeated Aqueous Flooding from the Cerberus Fossae: Evidence for Very Recently Extant, Deep Groundwater on Mars. *Icarus* **159**, 53–73 (2002).
17. Jaeger, W. L., Keszthelyi, L. P., McEwen, a. S., Dundas, C. M. & Russell, P. S. Athabasca Valles, Mars: a lava-draped channel system. *Science (New York, N.Y.)* **317**, 1709–11 (2007).
18. Burr, D. M., Mcewen, A. S. & Sakimoto, S. E. H. Recent aqueous floods from the Cerberus Fossae, Mars. *Geophysical Research Letters* **29**, 2–5 (2002).
19. Murray, J. B. *et al.* Evidence from the Mars Express High Resolution Stereo Camera for a frozen sea close to Mars' equator. *Letters to Nature* **434**, 352–355 (2005).
20. Page, D. P. Comment on "Athabasca Valles, Mars: A Lava-Draped Channel System". *Science* **320**, 2007–2008 (2008).
21. Balme, M. R., Gallagher, C. J., Page, D. P., Murray, J. B. & Muller, J.-P. Sorted stone circles in Elysium Planitia, Mars: Implications for recent martian climate. *Icarus* **200**, 30–38 (2009).
22. Morgan, G. A., Campbell, B. A., Carter, L. M. & Plaut, J. J. Evidence for the episodic erosion of the Medusae Fossae Formation preserved within the youngest volcanic province on Mars. *Geophysical Research Letters* 7336–7342, doi: 10.1002/2015GL065017. Received (2015).
23. Chevrier, V. F. & Altheide, T. S. Low temperature aqueous ferric sulfate solutions on the surface of Mars. *Geophysical Research Letters* **35**, L22101 (2008).
24. Chevrier, V. F. & Rivera-Valentin, E. G. Formation of recurring slope lineae by liquid brines on present-day Mars. *Geophysical Research Letters* **39**, L21202 (2012).
25. Altheide, T. S., Chevrier, V. F., Nicholson, C. & Denson, J. Experimental investigation of the stability and evaporation of sulfate and chloride brines on Mars. *Earth and Planetary Science Letters* **282**, 69–78 (2009).
26. Ojha, L. *et al.* Spectral evidence for hydrated salts in recurring slope lineae on Mars. *Nature Geoscience*, doi: 10.1038/ngeo2546 (2015).
27. Hurowitz, J. a. & McLennan, S. M. A ~3.5 Ga record of water-limited, acidic weathering conditions on Mars. *Earth and Planetary Science Letters* **260**, 432–443 (2007).
28. Dreibus, G. & Wanke, H. Mars, a volatile-rich planet. *Journal of Chemical Information and Modeling* **20**, 367–381 (1985).
29. Taylor, G. J. The bulk composition of Mars. *Chemie der Erde - Geochemistry* **73**, 401–420 (2013).
30. Karunatillake, S., McLennan, S. M. & Herkenhoff, K. E. Regional and grain size influences on the geochemistry of soil at Gusev crater, Mars. *Journal of Geophysical Research* **115**, E00F04 (2010).
31. McSween, H. Y. *et al.* Mineralogy of volcanic rocks in Gusev Crater, Mars: Reconciling Mössbauer, Alpha Particle X-Ray Spectrometer, and Miniature Thermal Emission Spectrometer spectra. *Journal of Geophysical Research* **113**, 1–14 (2008).
32. Hurowitz, J. A., McLennan, S. M., McSween, H. Y., DeSouza, P. a. & Klingelhöfer, G. Mixing relationships and the effects of secondary alteration in the Wishstone and Watchtower Classes of Husband Hill, Gusev Crater, Mars. *Journal of Geophysical Research* **111**, E12S14 (2006).
33. Ming, D. W. *et al.* Geochemical properties of rocks and soils in Gusev Crater, Mars: Results of the Alpha Particle X-Ray Spectrometer from Cumberland Ridge to Home Plate. *Journal of Geophysical Research* **113**, E12S39 (2008).
34. Balme, M. R. & Gallagher, C. An equatorial periglacial landscape on Mars. *Earth and Planetary Science Letters* **285**, 1–15 (2009).
35. Jaeger, W. L. *et al.* Emplacement of the youngest flood lava on Mars: A short, turbulent story. *Icarus* **205**, 230–243 (2010).
36. Spohn, T., Breuer, D. & Johnson, T. *Encyclopedia of the Solar System*, 3rd Edition. (2014).
37. Ruff, S. W. & Christensen, P. R. Bright and dark regions on Mars: Particle size and mineralogical characteristics based on Thermal Emission Spectrometer data. *Journal of Geophysical Research* **107**, 5127 (2002).
38. Nesbitt, H. W. & Wilson, R. E. Recent chemical weathering of basalts. *American Journal of Science* **292**, 740–777 (1992).
39. Sigurdur, R. & Gislason, S. A. Dissolution of primary basaltic minerals in natural waters: saturation state and kinetics. *Chemical Geology* **105**, 117–135 (1993).
40. Baratoux, D. *et al.* Petrological constraints on the density of the Martian crust. 1707–1727, doi: 10.1002/2014JE004642 (2014).
41. Hartmann, W. K. & Neukum, G. Cratering chronology and the evolution of Mars. *Space Science Reviews* **96**, 165–194 (2001).
42. Putzig, N., Mellon, M., Kretke, K. & Arvidson, R. Global thermal inertia and surface properties of Mars from the MGS mapping mission. *Icarus* **173**, 325–341 (2005).
43. Jones, E., Caprarelli, G., Mills, F., Doran, B. & Clarke, J. An Alternative Approach to Mapping Thermophysical Units from Martian Thermal Inertia and Albedo Data Using a Combination of Unsupervised Classification Techniques. *Remote Sensing* **6**, 5184–5237 (2014).
44. Newsom, H. E. *et al.* Geochemistry of Martian soil and bedrock in mantled and less mantled terrains with gamma ray data from Mars Odyssey. *Journal of Geophysical Research* **112**, E03S12 (2007).
45. Yen, A. S. *et al.* An integrated view of the chemistry and mineralogy of Martian soils. *Nature* **436**, 49–54 (2005).
46. McSween, H. Y., McGlynn, I. O. & Rogers, a. D. Determining the modal mineralogy of Martian soils. *Journal of Geophysical Research* **115**, E00F12 (2010).
47. Karunatillake, S. *et al.* Sulfates hydrating bulk soil in the Martian low and middle latitudes. *Geophysical Research Letters* **41**, 7987–7996 (2014).
48. Elkins-Tanton, L. T., Hess, P. C. & Parmentier, E. M. Possible formation of ancient crust on Mars through magma ocean processes. *Journal of Geophysical Research E: Planets* **110**, 1–11 (2005).
49. Balta, J. B. & McSween, H. Y. Water and the composition of Martian magmas. *Geology* **41**, 1115–1118 (2013).
50. Auzende, A. L. *et al.* Element partitioning between magnesium silicate perovskite and ferropericlae: New insights into bulk lower-mantle geochemistry. *Earth and Planetary Science Letters* **269**, 164–174 (2008).
51. McSween, H. Y., Taylor, G. J. & Wyatt, M. B. Elemental composition of the Martian crust. *Science* **324**, 736–9 (2009).
52. Karunatillake, S. *et al.* Martian Case Study of Multivariate Correlation and Regression with Planetary Datasets. *Earth, Moon, and Planets* **108**, 253–273 (2012).
53. Karunatillake, S. *et al.* Recipes for Spatial Statistics with Global Datasets: A Martian Case Study. *Journal of Scientific Computing* **46**, 439–451 (2011).
54. Miller, J. N. & Miller, J. C. *Statistics and Chemometrics for Analytical Chemistry*. (Pearson, 2010).
55. Rogers, a. D. & Nazarian, a. H. Evidence for Noachian flood volcanism in Noachis Terra, Mars, and the possible role of Hellas impact basin tectonics. *Journal of Geophysical Research: Planets* **118**, 1094–1113 (2013).

Acknowledgements

We acknowledge NASA Mars Data Analysis Program (MDAP) grant NNX13A198G, the LA Space Grant Consortium REA grant 115-40-4139 and Graduate Student Research Award (GSRA) NNX15AH82H, and the LSU Chancellor's Aide student Scholarship without which none of this research would have been possible. We acknowledge Charles Everhardt and Rory Bentley for their hard work with crater counting and image analysis. Thank you to Lorrie Carnes and Don Hood for providing editorial revisions. Also, thank you to the reviewers of this manuscript James Dohm and a second reviewer who wished to remain anonymous. Their comments and revisions forced this work to mature to be the most scientifically robust that it could be.

Author Contributions

D.S. did research, contributed to analysis, formatted all figures, and wrote the manuscript. S.K. contributed considerably to the writing of the manuscript, and guided the analytical work as D.S.'s PhD dissertation adviser. G.K. produced Figure 4 and underlying analyses, while also contributing to writing. J.S. provided guidance for the construction of Figure 2, along with insight on volcanic processes on Mars. A.C. provided and interpreted data to be used in the analysis within the manuscript, especially on developing optimal sample categories. T.J. contributed to the initial research and analysis. All co-authors provided detailed and conceptual revisions to the manuscript, led by J.W. and J.H.

Additional Information

Competing financial interests: The authors declare no competing financial interests.

How to cite this article: Susko, D. *et al.* A record of igneous evolution in Elysium, a major martian volcanic province. *Sci. Rep.* 7, 43177; doi: 10.1038/srep43177 (2017).

Publisher's note: Springer Nature remains neutral with regard to jurisdictional claims in published maps and institutional affiliations.



This work is licensed under a Creative Commons Attribution 4.0 International License. The images or other third party material in this article are included in the article's Creative Commons license, unless indicated otherwise in the credit line; if the material is not included under the Creative Commons license, users will need to obtain permission from the license holder to reproduce the material. To view a copy of this license, visit <http://creativecommons.org/licenses/by/4.0/>

© The Author(s) 2017